Heterogeneity of SSTR2 Expression Assessed by ^{68}Ga-DOTATOC PET/CT Using Coefficient of Variation in Patients with Neuroendocrine Tumors

Rosa Fonti[1,2], Mariarosaria Panico[1,2], Sara Pellegrino[2], Alessandro Pulcrano[2], Luisa Alessia Vastarella[2], Armin Hakkak Moghadam Torbati[2], Mario Giuliano[3,4], Giovannella Palmieri[4], Sabino De Placido[3,4], and Silvana Del Vecchio[2]

[1]*Institute of Biostructures and Bioimages, National Research Council, Naples, Italy;* [2]*Department of Advanced Biomedical Sciences, University of Naples "Federico II," Naples, Italy;* [3]*Department of Clinical Medicine and Surgery, University of Naples "Federico II," Naples, Italy; and* [4]*CRCTR Coordinating Rare Tumors Reference Center of Campania Region, AOU "Federico II," Naples, Italy*

High levels of somatostatin receptor subtype 2 (SSTR2) are a prerequisite for therapy with unlabeled or labeled somatostatin analogs. However, it is still unclear how the heterogeneity of SSTR2 expression may affect tumor response to therapy. The aim of our study was to test the ability of an imaging parameter such as coefficient of variation (CoV) derived from PET/CT with ^{68}Ga-peptides in the evaluation and quantification of the heterogeneity of SSTR2 expression within primary and metastatic lesions of patients with neuroendocrine tumors. **Methods:** Thirty-eight patients with pathologically proven neuroendocrine tumors who underwent ^{68}Ga-DOTATOC PET/CT were studied. Primary tumors were localized in the gastroenteropancreatic, bronchopulmonary, and other anatomic districts in 25, 7, and 6 patients, respectively. Malignant lesions were segmented using an automated contouring program and an SUV threshold of more than 2.5 or, in the case of liver lesions, a threshold of 30% of the SUV_{max}. The imaging parameters SUV_{mean}, CoV, SUV_{max}, receptor-expressing tumor volume, and total lesion receptor expression were obtained for each lesion. SUV_{mean}, CoV, and SUV_{max} were also obtained for representative volumes of normal liver and spleen, as well as for the whole pituitary gland. **Results:** In total, 107 lesions were analyzed, including 35 primary tumors, 32 metastatic lymph nodes, and 40 distant metastases. Average CoVs were 0.49 ± 0.20 for primary tumors, 0.57 ± 0.26 for lymph node metastases, and 0.44 ± 0.20 for distant metastases. The CoVs of malignant lesions were up to 4-fold higher than those of normal tissues ($P \leq 0.0001$). Among malignant lesions, the highest CoV was found for bone metastases (0.68 ± 0.20), and it was significantly greater than that of primary lesions ($P = 0.01$) and liver metastases ($P < 0.0001$). On the other hand, the lowest CoV was found for liver lesions (0.32 ± 0.07), probably because of the high background uptake. **Conclusion:** Our findings indicate that the heterogeneity of uptake, reflecting that of SSTR2, varies with the type and site of malignant lesions as assessed by CoVs obtained from ^{68}Ga-DOTATOC PET/CT scans. These observations may be related to different biologic characteristics of tumor lesions in the same patient—differences that may affect their response to treatment with both labeled and unlabeled somatostatin analogs.

Key Words: somatostatin receptor 2; heterogeneity; coefficient of variation; ^{68}Ga-peptide PET/CT; neuroendocrine tumors

J Nucl Med 2022; 63:1509–1514
DOI: 10.2967/jnumed.121.262928

Received Jul. 27, 2021; revision accepted Feb. 12, 2022.
For correspondence or reprints, contact Silvana Del Vecchio (delvecc@unina.it).
Published online Mar. 10, 2022.

Neuroendocrine neoplasms are a heterogeneous group of rare tumors arising from the diffuse neuroendocrine cell system and include both well-differentiated neuroendocrine tumors (NETs) and poorly differentiated carcinomas. Grading of NETs is essentially based on the rate of proliferation as assessed by Ki-67 staining (*1*). A common property of well-differentiated NETs is overexpression of somatostatin receptors (SSTRs), which constitute a target for therapy with unlabeled and β-emitter–conjugated somatostatin analogs (*2,3*).

SSTRs belong to the large family of G protein–coupled receptors that, on binding with their specific ligands, activate guanosine triphosphate–binding proteins, which, in turn, propagate a signaling cascade using different second-messenger systems (*4,5*). Of the 5 known SSTR subtypes, 1–5, the SSTR2 subtype is the most widely distributed in normal tissues and human tumors (*6*). High levels of SSTR2 have been found mainly in grade 1 and grade 2 NETs, for which a heterogeneous pattern of expression was also observed (*7,8*). Although previous studies showed that high levels of SSTR2 could predict a good response to therapy with somatostatin analogs and a prolonged survival (*7,8*), it is still unclear how the heterogeneity of SSTR2 expression within a lesion or among different lesions in the same patient may affect tumor response to therapy and clinical outcome.

SSTR2 displays a complex temporal and tissue-specific pattern of expression involving several growth and transcriptional factors, hormones, inflammatory cytokines, specific ligands, and microenviromental conditions (*4,9*). More recently, a growing body of evidence indicates that SSTR2 expression can be regulated by epigenetic mechanisms (*10,11*) such as DNA methylation and histone acetylation. Furthermore, upregulation of SSTR2 has been reported to occur through activation of NF-κB and MEK signaling pathways in a model of Epstein–Barr infection of nasopharyngeal carcinoma cells (*12*).

To test the predictive and prognostic value of intratumoral heterogeneity of SSTR2 expression and its possible role in the prediction and evaluation of peptide receptor radionuclide therapy response, some authors adopted a radiomic approach to extract several features from PET/CT scans acquired with ^{68}Ga-labeled analogs (*13–17*). In particular, one of these studies (*13*) found that 4 parameters—that is, entropy, correlation, short-zone emphasis, and homogeneity—were able to predict both progression-free survival and overall survival in patients who were candidates for peptide receptor radionuclide therapy. Furthermore, receptor-expressing tumor volume (RETV) could predict overall survival, whereas SUV_{max} and SUV_{mean} did not

correlate with survival. In another study (*16*), specific texture features derived from ^{68}Ga-DOTATOC and ^{18}F-FDG PET/CT, including intensity variability, size zone variability, zone percentage, entropy, homogeneity, dissimilarity, and coefficient of variation (CoV), were actually able to predict size, angioinvasion, and lymph node involvement in pancreatic NETs.

Among the texture features for the assessment of tumor heterogeneity, CoV is a simple and easy-to-calculate first-order parameter that indicates the percentage variability in SUV_{mean} within the tumor volume, reflecting the heterogeneity of tracer distribution and hence SSTR variability in ^{68}Ga-peptide examinations.

Although we are aware that radiomics is a powerful tool to characterize tumor heterogeneity and to extract clinically relevant subvisual information from PET images, the aim of the present study was to test the ability of a first-order parameter such as CoV derived from ^{68}Ga-peptide PET/CT scans to quantify the heterogeneity of SSTR2 expression within primary and metastatic lesions of NET patients.

MATERIALS AND METHODS

Patients

We studied 38 patients (25 men, 13 women; mean age, 60 ± 14 y; age range, 29–80 y) with pathologically proven NETs who underwent ^{68}Ga-DOTATOC PET/CT at our institution. The study was approved by the institutional review board, and all subjects signed an informed consent form. The patients were examined at the time of first diagnosis or during the course of disease, and 6 of them were reexamined during follow-up; in total, therefore, 44 ^{68}Ga-DOTATOC scans were obtained and evaluated. The primary tumor was localized in the gastroenteropancreatic district (25 patients: 16 pancreas, 6 midgut, and 3 mesentery), in the bronchopulmonary district (7 patients), or in other anatomic districts (6 patients). Tumor grade and Ki-67 proliferation index were available for 30 patients. Among them, 11 patients were classified as grade 1, 16 as grade 2, and 3 as grade 3; Ki-67 was less than 3% in 11 patients, between 3% and 20% in 16, and more than 20% in 3 (*1*). Ten patients had primary tumor only, 9 patients had lymph node but not distant metastases, and 19 patients had distant metastases with or without lymph node metastases. The patient characteristics are shown in Table 1. Seventeen ^{68}Ga-DOTATOC PET/CT scans were obtained for patients who had previously undergone surgery. When administered, previous treatments such as chemotherapy, temozolomide, or everolimus were discontinued at least 6 mo before the PET/CT scan. Furthermore, 18 scans were obtained for patients under treatment with somatostatin analogs using a standard regimen (30 mg intramuscularly once every 4 wk), because to avoid disease progression, discontinuation of therapy was not clinically recommended. In these patients, somatostatin analogs were administered on average 12.9 ± 7.6 (SD) days before the PET/CT scan, whereas the other patients receiving somatostatin analogs discontinued somatostatin analogs more than 1 mo before the scan.

TABLE 1
Patient Characteristics

Characteristic	Data
No. of patients	38
Age (y)	
Mean ± SD	60 ± 14
Range	29–80
Sex	
Female	13 (34%)
Male	25 (66%)
Type of NET	
Gastroenteropancreatic	25 (66%)
Bronchopulmonary	7 (18%)
Other	6 (16%)
Grade	
1	11 (29%)
2	16 (42%)
3	3 (8%)
Not determined	8 (21%)
Ki-67 (%)	
<3	11 (29%)
3–20	16 (42%)
>20	3 (8%)
Not determined	8 (21%)
Lesion sites per patient	
PT only	10 (26%)
PT + LNM	6 (16%)
PT + DM	6 (16%)
PT + LNM + DM	6 (16%)
LNM only	3 (8%)
DM only	3 (8%)
LNM + DM	4 (10%)

PT = primary tumor; LNM = lymph node metastases; DM = distant metastases.
Data are number, except for age.

^{68}Ga-DOTATOC Labeling

The radiopharmaceutical was prepared using a commercially available kit (SomaKit TOC; Advanced Accelerator Application) containing DOTATOC (edotreotide), a somatostatin analog with a high affinity for SSTR2. Edotreotide labeling was performed following the manufacturer's instructions. Briefly, ^{68}Ga-chloride eluted directly from a ^{68}Ge/^{68}Ga generator (Eckert and Ziegler Radiopharma GmbH) was added to 40 μg of peptide. The solution was immediately buffered and heated to 95°C for 7 min using a hot plate. Finally, the product was cooled at room temperature before use. All steps were performed under sterile conditions, and the final product was subjected to thin-layer chromatography to verify labeling efficiency. In all labeling procedures, the percentages of free and colloidal ^{68}Ga were no more than 2% and 3%, respectively.

^{68}Ga-DOTATOC PET/CT Study

Sixty minutes after intravenous administration of ^{68}Ga-DOTATOC (135 ± 25 MBq), patients underwent PET/CT using an Ingenuity TF scanner (Philips Healthcare). CT imaging was performed using the following parameters: 120 kV, 80 mA, a 0.8-s rotation time, and a pitch of 1.5. The PET scan was acquired in 3-dimensional mode, from the top of the skull to the upper thigh (3 min per bed position), at 6–8 bed positions per patient, depending on height. Images were iteratively reconstructed with ordered-subsets expectation maximization algorithm. Attenuation-corrected emission data were obtained using filtered backprojection of CT-reconstructed images. The resulting transaxial, sagittal, and coronal PET, CT, and fusion images were preliminarily examined using the Ingenuity TF software.

^{68}Ga-DOTATOC PET/CT Image Analysis

Images were transferred in DICOM format to a workstation equipped with the LIFEx program (*18*). All focal areas not attributable to physiologic uptake of ^{68}Ga-DOTATOC that showed morphologic or structural alterations on the corresponding CT images were considered positive. In cases of multiple liver or bone metastases, the lesion with the highest SUV_{max} was analyzed, whereas coalescent lymph nodes were considered a single lesion. A volume of interest (VOI) for each positive lesion was obtained by drawing a 3-dimensional region around the lesion using an automatic segmentation method (*19,20*) that groups all spatially connected voxels within a predefined threshold. In particular, an SUV threshold of more than 2.5 was used for all lesions on the basis of the mean SUV_{max} of the mediastinal blood pool plus 2 SDs. The exception was liver metastases, for which, because of the high physiologic liver uptake, a threshold of 30% of the SUV_{max} was used to avoid inclusion of normal parenchyma in the VOI (*21,22*). In addition, the accuracy of tumor delineation was confirmed on the corresponding CT images. By computed analysis of each VOI, the following parameters were obtained: SUV_{mean}, CoV (SD divided by SUV_{mean}), SUV_{max}, RETV, and total lesion receptor expression (TLRE), obtained by multiplying SUV_{mean} by RETV. In addition to tumor lesions, normal organs with high physiologic uptake were also analyzed, thus obtaining SUV_{mean}, CoV, and SUV_{max} in representative volumes of liver and spleen (using VOIs of the same size), as well as in the entire pituitary gland. Representative images of VOIs drawn around malignant lesions and within normal tissues are shown in Figure 1.

Statistical Analysis

Statistical analysis was performed using MedCalc software for Microsoft Windows, version 10.3.2.0. A P value of less than 0.05 was considered statistically significant. The Student t test was used to compare means of unpaired data.

RESULTS

Forty-four ^{68}Ga-DOTATOC PET/CT scans were acquired for 38 NET patients. In total, 107 lesions were analyzed, including 35 primary tumors (27 gastroenteropancreatic, 5 bronchopulmonary, and 3 in other anatomic districts), 32 lymph node metastases (20 regional and 12 nonregional), and 40 distant metastases (21 in the liver, 10 in the bones, and 9 in other anatomic sites [2 in the pancreas, 3 in the spleen, 2 in the peritoneum, 1 in the thyroid, and 1 in the retroperitoneum]) as shown in Table 2. The imaging parameters SUV_{mean}, CoV, SUV_{max}, RETV, and TLRE obtained for primary lesions, lymph node metastases, and distant metastases are shown in Table 3. In addition to tumor lesions, normal organs with high physiologic uptake such as liver, spleen, and pituitary gland were also analyzed, and the SUV_{mean}, CoV, and SUV_{max} are reported in Table 4.

We first examined the effects of treatment with somatostatin analogs on uptake in both tumor lesions and normal tissues by comparing the SUV_{max} obtained for patients undergoing (n = 18) or not undergoing (n = 26) therapy at the time of the ^{68}Ga-DOTATOC scan. As shown in Table 5, no statistically significant difference in the SUV_{max} for malignant lesions (primary tumors, lymph node metastases, and distant metastases) was found between treated and untreated patients. In contrast, uptake was significantly reduced in the normal liver ($P < 0.0001$), spleen ($P < 0.0001$), and pituitary gland ($P < 0.02$) of treated patients. These data indicate that administration of somatostatin analogs using a standard regimen reduces physiologic uptake of ^{68}Ga-DOTATOC in normal organs without affecting uptake in malignant lesions. Similarly, neither SUV_{mean} nor CoV in primary lesions (P = 0.3515 and 0.2718, respectively), lymph node metastases (P = 0.4497 and 0.0748, respectively), and distant metastases (P = 0.1068 and 0.2128, respectively) statistically differed between patients under treatment and those who were not. Therefore, the imaging parameters were analyzed in all patients as a whole group.

SUV_{mean} for primary lesions, lymph node metastases, and distant metastases was 8.70 ± 7.53, 8.38 ± 4.10, and 13.72 ± 9.90, respectively (Table 3). There was no statistically significant difference in SUV_{mean} between primary lesions and lymph node metastases (P = 0.8507), whereas both were significantly lower than distant metastases (P = 0.0170 and 0.0056, respectively). Moreover, CoVs for primary lesions, lymph node metastases, and distant metastases were 0.49 ± 0.20, 0.57 ± 0.26, and 0.44 ± 0.20, respectively (Table 3). There were no statistically significant differences in CoV between primary lesions and lymph node

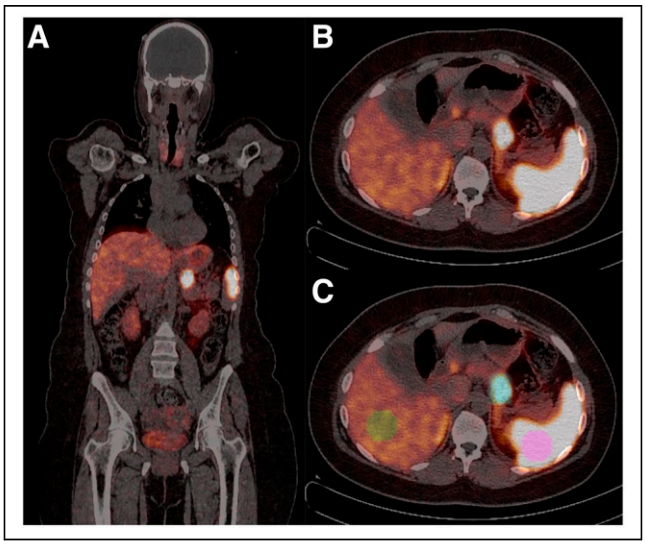

FIGURE 1. ^{68}Ga-DOTATOC PET/CT in patient with pancreatic NET. (A) Coronal image showing primary tumor. (B and C) Transaxial images of same section without (B) and with (C) overlay of VOIs drawn around primary tumor (blue VOI), within normal liver (green VOI), and within normal spleen (pink VOI).

TABLE 2
Type and Number of Lesions Analyzed on ^{68}Ga-DOTATOC PET/CT Images

Lesion type	*n*
Primary tumor	35
Gastroenteropancreatic tract	27
Bronchopulmonary tract	5
Other sites	3
Lymph node metastases	32
Regional basins	20
Nonregional basins	12
Distant metastases	40
Liver	21
Bone	10
Other sites	9
Total lesions	107

TABLE 3
Imaging Parameters Obtained by ^{68}Ga-DOTATOC PET/CT Analysis of Primary Tumors, Lymph Node Metastases, and Distant Metastases

Parameter	Mean ± SD	Median	Range	*P**
SUV_{max}				
Primary tumor	24.10 ± 19.51	16.60	4.78–88.31	T vs. N = 0.4559
Lymph node metastases	27.77 ± 20.51	21.51	3.00–82.04	N vs. M = 0.2256
Distant metastases	34.99 ± 27.89	28.26	3.98–115.55	M vs. T = 0.0573
SUV_{mean}				
Primary tumor	8.70 ± 7.53	6.86	3.29–42.72	T vs. N = 0.8507
Lymph node metastases	8.38 ± 4.10	8.05	1.41–18.31	N vs. M = 0.0056
Distant metastases	13.72 ± 9.90	12.44	1.68–43.41	M vs. T = 0.0170
CoV				
Primary tumor	0.49 ± 0.20	0.51	0.17–0.95	T vs. N = 0.1730
Lymph node metastases	0.57 ± 0.26	0.58	0.10–1.07	N vs. M = 0.0253
Distant metastases	0.44 ± 0.20	0.39	0.14–1.00	M vs. T = 0.3260
RETV (mL)				
Primary tumor	25.07 ± 34.75	10.69	2.43–178.24	T vs. N = 0.0879
Lymph node metastases	13.26 ± 17.42	7.04	0.80–82.04	N vs. M = 0.0044
Distant metastases	33.68 ± 36.04	18.97	2.11–136.25	M vs. T = 0.2972
TLRE (g)				
Primary tumor	309.83 ± 813.83	63.29	15.80–4766.19	T vs. N = 0.2616
Lymph node metastases	142.56 ± 195.34	71.25	2.99–766.21	N vs. M = 0.0028
Distant metastases	601.23 ± 816.25	258.38	3.56–2908.85	M vs. T = 0.1268

*Unpaired *t* test (T = primary tumor; N = lymph node metastases; M = distant metastases).

metastases ($P = 0.1730$) or distant metastases ($P = 0.3260$), whereas lymph node metastases had a significantly higher CoV than did distant metastases ($P = 0.0253$).

In a further analysis, distant metastases were divided into 3 subgroups, including liver, bone, and other metastatic lesions, and for each subgroup SUV_{mean} and CoVs were determined (Table 6). The average SUV_{mean} for liver, bone, and other metastatic lesions was 17.09 ± 11.61, 9.61 ± 6.40, and 10.45 ± 5.67, respectively. No statistically significant differences in SUV_{mean} were found among the 3 subgroups of distant metastases. The CoVs for liver, bone, and other metastatic lesions were 0.32 ± 0.07, 0.68 ± 0.20, and 0.47 ± 0.15, respectively. Bone metastases had a significantly higher CoV than either liver lesions ($P < 0.0001$) or metastases at

TABLE 4
Imaging Parameters Obtained by ^{68}Ga-DOTATOC PET/CT Analysis of Normal Organs with High Physiologic Tracer Uptake Such as Liver, Spleen, and Pituitary Gland

Parameter	Mean ± SD	Median	Range
SUV_{max}			
Liver	9.07 ± 3.45	9.37	3.12–19.90
Spleen	24.56 ± 11.61	21.89	5.23–46.35
Pituitary gland	6.03 ± 2.58	5.88	0.99–12.00
SUV_{mean}			
Liver	5.94 ± 2.60	5.82	1.84–11.27
Spleen	18.48 ± 9.71	18.89	3.00–35.63
Pituitary gland	3.95 ± 0.74	3.89	1.13–5.30
CoV			
Liver	0.16 ± 0.07	0.14	0.06–0.44
Spleen	0.16 ± 0.09	0.14	0.06–0.56
Pituitary gland	0.29 ± 0.11	0.26	0.09–0.63

TABLE 5
SUV_{max} in Malignant Lesions and Normal Tissues in Patients Treated or Not Treated with Somatostatin Analogs

Tissue type	No SSA therapy	SSA therapy	*P*
Primary lesion	25.08 ± 22.49	22.44 ± 13.75	NS
Lymph node metastasis	22.22 ± 22.25	31.57 ± 18.89	NS
Distant metastasis	22.49 ± 13.97	40.34 ± 30.74	NS
Normal liver	10.76 ± 3.11	6.55 ± 2.21	<0.0001
Normal spleen	32.40 ± 8.92	15.49 ± 6.69	<0.0001
Normal pituitary	7.03 ± 2.18	4.48 ± 2.43	<0.02

NS = not significant.
Data are mean ± SD.

TABLE 6
Imaging Parameters Obtained by ^{68}Ga-DOTATOC PET/CT Analysis of Liver, Bone, and Other Distant Metastases

Parameter	Mean ± SD	Median	Range	*P**
SUV_{max}				
Liver metastases	37.98 ± 31.13	28.49	6.87–115.55	L vs. B = 0.8234
Bone metastases	35.33 ± 29.61	18.83	3.98–94.90	B vs. O = 0.5038
Other metastases	27.61 ± 17.27	34.72	5.36–51.79	O vs. L = 0.3586
SUV_{mean}				
Liver metastases	17.09 ± 11.61	13.40	4.47–43.41	L vs. B = 0.0684
Bone metastases	9.61 ± 6.40	6.19	1.68–21.85	B vs. O = 0.7651
Other metastases	10.45 ± 5.67	14.23	3.43–16.54	O vs. L = 0.0600
CoV				
Liver metastases	0.32 ± 0.07	0.33	0.14–0.46	L vs. B < 0.0001
Bone metastases	0.68 ± 0.20	0.61	0.42–1.00	B vs. O = 0.0269
Other metastases	0.47 ± 0.15	0.50	0.20–0.65	O vs. L = 0.0006

*Unpaired *t* test (L = liver metastasis; B = bone metastases; O = other metastases).

other sites ($P = 0.0269$). A significant difference was also found between the CoVs for liver and the CoVs for other metastatic lesions ($P = 0.0006$). Therefore, the greatest heterogeneity of uptake reflecting SSTR expression was found in bone lesions, compared with the other distant metastases.

Furthermore, the CoV was significantly higher for bone metastases than for primary lesions ($P = 0.0132$) but did not significantly differ from that for lymph node metastases ($P = 0.2330$). In contrast, the CoV was significantly lower for liver metastases than for primary lesions ($P = 0.0005$) or lymph node metastases ($P = 0.0001$). On the other hand, no statistically significant differences in CoV were found between metastases at other sites and primitive lesions ($P = 0.8327$) or lymph node metastases ($P = 0.3138$). Finally, as expected, the mean CoV was significantly higher ($P \leq 0.0001$) for primary lesions, lymph node metastases, and distant metastases than for normal liver, spleen, and pituitary gland.

Values of conventional parameters such as SUV_{max} and volumetric parameters such as RETV and TLRE obtained for tumor lesions are shown in Table 3. SUV_{max} was 24.10 ± 19.51 for primary lesions, 27.77 ± 20.51 for lymph node metastases, and 34.99 ± 27.89 for distant metastases. No statistically significant differences in SUV_{max} were found among these 3 groups of lesions, although the SUV_{max} of distant metastases tended to be higher than that of primary lesions ($P = 0.0573$). RETV and TLRE were 25.07 ± 34.75 and 309.83 ± 813.83, respectively, for primary lesions; 13.26 ± 17.42 and 142.56 ± 195.34, respectively, for lymph node metastases; and 33.68 ± 36.04 and 601.23 ± 816.25, respectively, for distant metastases. RETV and TLRE were significantly greater for distant metastases than for lymph node metastases ($P = 0.0044$ and 0.0028, respectively), whereas RETV and TLRE did not significantly differ between primary lesions and lymph node metastases ($P = 0.0879$ and 0.2616, respectively) or distant metastases ($P = 0.2972$ and 0.1268, respectively).

DISCUSSION

Our study showed that all malignant lesions had up to a 4-fold higher CoV than normal tissues. In particular, the highest CoV was found for bone metastases, followed by lymph node metastases and primary lesions, reflecting the variable expression of SSTR depending on type and site of lesion. These findings suggest that, because of receptor heterogeneity among lesions, the biologic behavior of tumor cells may vary at different sites, leading to different patterns of tumor growth and progression and to different responses to targeted therapy with somatostatin analogs.

On the other hand, liver metastases, despite having the highest uptake, showed the lowest CoV among the 3 groups of distant metastases. The reason could be that metastatic cells infiltrate and proliferate within a tissue with a high and homogeneous physiologic uptake such as normal liver. In fact, to avoid inclusion of normal parenchyma in the tumor VOI, we used a percentage segmentation threshold different from that of all other lesions, and the accuracy of the tumor-contouring procedure was carefully checked on the corresponding CT images. However, it cannot be ruled out that normal liver parenchyma may be interspersed with clusters of metastatic cells within the lesion.

Previous studies evaluated the heterogeneity of SSTR expression by texture analysis determining the prognostic value of several texture parameters such as entropy and homogeneity in NET patients (*23,24*). In our study, we used a simple first-order parameter such as CoV that was able to reveal and quantitate the heterogeneity of receptor expression in malignant lesions, depending on their type and site. Furthermore, our observations may provide methodologic clues for texture analysis of NETs since metastatic lesions in different districts cannot be analyzed together because they can have a different predictive value on tumor response and final outcome due to significantly different heterogeneity. Moreover, using a texture analysis approach, the repeatability and reproducibility of texture features are a major issue. In this respect, CoV measurements depend on the same factors as those that affect conventional parameters such as SUV_{max} and SUV_{mean}, and we used an automated contouring program to standardize the procedure as much as possible.

The site-dependent pattern of SSTR2 heterogeneity in malignant lesions may be caused by the different microenvironmental conditions at the various sites. Accumulating evidence indeed indicates that a dynamic cross-talk exists between NET cells and tumor stroma, since NET cells produce a large spectrum of proangiogenic

and profibrotic factors inducing a high intratumoral microvascular density and fibrotic complications whereas stromal cells such as fibroblasts, endothelial cells, and inflammatory cells produce several growth factors and cytokines that can modulate proliferation and likely receptor expression in NET cells (*9*).

In our study, we also evaluated the possible effect of therapy with somatostatin analogs on the uptake of ^{68}Ga-peptide in tumor lesions and normal tissues. We showed that, between treated and untreated patients, there were no significant differences in SUV_{max} for primary lesions, lymph node metastases, and distant metastases, whereas SUV_{max} was significantly lower for normal liver, spleen, and pituitary gland in treated patients than in untreated patients. These findings indicate that administration of standard doses of somatostatin analogs reduces uptake of ^{68}Ga-peptide in high-capacity, low-affinity compartments such as normal liver and spleen but has no detectable effects on uptake in low-capacity, high-affinity compartments such as malignant lesions. It is likely that the standard doses of peptide usually prescribed to NET patients do not reach the large excess of cold peptide probably needed to compete with ^{68}Ga-peptide for receptor binding in tumor cells. On the other hand, it is well known that binding of somatostatin analogs to SSTR2 is followed by receptor internalization and that this process may reduce receptor density on the plasma membrane. However, there is evidence that prolonged treatment with somatostatin analogs may cause receptor upregulation (*5*), probably depending on cell context and microenviromental conditions. These findings taken together may be useful in clinical practice, as discontinuation of therapy with somatostatin analogs in patients undergoing PET/CT with ^{68}Ga peptides might be avoided without affecting the results of the diagnostic scan.

CONCLUSION

Our study showed that a simple parameter obtained by ^{68}Ga-DOTATOC PET/CT image analysis such as CoV allows the evaluation of uptake heterogeneity in tumor lesions in different anatomic districts. The heterogeneity of uptake reflects that of SSTR expression and may therefore be related to different biologic characteristics of tumor lesions in the same patient, potentially predicting a differential tumor response to treatment with both labeled and unlabeled somatostatin analogs.

DISCLOSURE

No potential conflict of interest relevant to this article was reported.

KEY POINTS

QUESTION: Can heterogeneity of SSTR2 expression easily be evaluated by ^{68}Ga-peptide PET/CT in a clinical context?

PERTINENT FINDINGS: Heterogeneity of SSTR2 was measured by CoV derived from ^{68}Ga-peptide PET/CT performed on NET patients. The highest CoV was found for bone metastases, followed by lymph node metastases and primary lesions.

IMPLICATIONS FOR PATIENT CARE: The heterogeneity of ^{68}Ga-DOTATOC uptake, reflecting that of SSTR2, varies with the type and site of malignant lesions and may affect the response to treatment with both labeled and unlabeled somatostatin analogs.

REFERENCES

1. Pavel M, Öberg K, Falconi M, et al. Gastroenteropancreatic neuroendocrine neoplasms: ESMO clinical practice guidelines for diagnosis, treatment and follow-up. *Ann Oncol.* 2020;31:844–860.
2. Strosberg J, El-Haddad G, Wolin E, et al. Phase 3 trial of ^{177}Lu-Dotatate for midgut neuroendocrine tumors. *N Engl J Med.* 2017;376:125–135.
3. Kong G, Hicks RJ. Peptide receptor radiotherapy: current approaches and future directions. *Curr Treat Options Oncol.* 2019;20:77.
4. Barnett P. Somatostatin and somatostatin receptor physiology. *Endocrine.* 2003;20:255–264.
5. Olias G, Viollet C, Kusserow H, Epelbaum J, Meyerhof W. Regulation and function of somatostatin receptors. *J Neurochem.* 2004;89:1057–1091.
6. Reubi JC, Waser B. Concomitant expression of several peptide receptors in neuroendocrine tumours: molecular basis for in vivo multireceptor tumour targeting. *Eur J Nucl Med Mol Imaging.* 2003;30:781–793.
7. Qian ZR, Li T, Ter-Minassian M, et al. Association between somatostatin receptor expression and clinical outcomes in neuroendocrine tumors. *Pancreas.* 2016;45:1386–1393.
8. Hu Y, Ye Z, Wang F, et al. Role of somatostatin receptor in pancreatic neuroendocrine tumor development, diagnosis, and therapy. *Front Endocrinol (Lausanne).* 2021;12:679000.
9. Cives M, Pelle' E, Quaresmini D, Rizzo FM, Tucci M, Silvestris F. The tumor microenvironment in neuroendocrine tumors: biology and therapeutic implications. *Neuroendocrinology.* 2019;109:83–99.
10. Klomp MJ, Dalm SU, de Jong M, Feelders RA. Hofland, Hofland LJ. Epigenetic regulation of somatostatin and somatostatin receptors in neuroendocrine tumors and other types of cancer. *Rev Endocr Metab Disord.* 2021;22:495–510.
11. Taelman VF, Radojewski P, Marincek N, et al. Upregulation of key molecules for targeted imaging and therapy. *J Nucl Med.* 2016;57:1805–1810.
12. Lechner M, Schartinger VH, Steele CD, et al. Somatostatin receptor 2 expression in nasopharyngeal cancer is induced by Epstein Barr virus infection: impact on prognosis, imaging and therapy. *Nat Commun.* 2021;12:117.
13. Werner RA, Lapa C, Ilhan H, et al. Survival prediction in patients undergoing radionuclide therapy based on intratumoral somatostatin-receptor heterogeneity. *Oncotarget.* 2017;8:7039–7049.
14. Önner H, Abdülrezzak U, Tutuş A. Could the skewness and kurtosis texture parameters of lesions obtained from pretreatment Ga-68 DOTA-TATE PET/CT images predict receptor radionuclide therapy response in patients with gastroenteropancreatic neuroendocrine tumors? *Nucl Med Commun.* 2020;41:1034–1039.
15. Weber M, Kessler L, Schaarschmidt B, et al. Treatment-related changes in neuroendocrine tumors as assessed by textural features derived from ^{68}Ga-DOTATOC PET/MRI with simultaneous acquisition of apparent diffusion coefficient. *BMC Cancer.* 2020;20:326.
16. Mapelli P, Partelli S, Salgarello M, et al. Dual tracer ^{68}Ga-DOTATOC and ^{18}F-FDG PET/computed tomography radiomics in pancreatic neuroendocrine neoplasms: an endearing tool for preoperative risk assessment. *Nucl Med Commun.* 2020;41:896–905.
17. Liberini V, Rampado O, Gallio E, et al. ^{68}Ga-DOTATOC-PET/CT-based radiomic analysis and PRRT outcome: a preliminary evaluation based on an exploratory radiomic analysis on two patients. *Front Med (Lausanne).* 2021;7:601853.
18. Nioche C, Orlhac F, Boughdad S, et al. LIFEx: a freeware for radiomic feature calculation in multimodality imaging to accelerate advances in the characterization of tumor heterogeneity. *Cancer Res.* 2018;78:4786–4789.
19. Fonti R, Larobina M, Del Vecchio S, et al. Metabolic tumor volume assessed by ^{18}F-FDG PET/CT for the prediction of outcome in patients with multiple myeloma. *J Nucl Med.* 2012;53:1829–1835.
20. Pellegrino S, Fonti R, Mazziotti E, et al. Total metabolic tumor volume by ^{18}F-FDG PET/CT for the prediction of outcome in patients with non-small cell lung cancer. *Ann Nucl Med.* 2019;33:937–944.
21. Fonti R, Conson M, Del Vecchio S. PET/CT in radiation oncology. *Semin Oncol.* 2019;46:202–209.
22. Liberini V, De Santi B, Rampado O, et al. Impact of segmentation and discretization on radiomic features in ^{68}Ga-DOTA-TOC PET/CT images of neuroendocrine tumor. *EJNMMI Phys.* 2021;8:21.
23. Bezzi C, Mapelli P, Presotto L, et al. Radiomics in pancreatic neuroendocrine tumors: methodological issues and clinical significance. *Eur J Nucl Med Mol Imaging.* 2021;48:4002–4015.
24. Saleh M, Bhosale PR, Yano M, et al. New frontiers in imaging including radiomics updates for pancreatic neuroendocrine neoplasms. *Abdom Radiol (NY).* October 23, 2020 [Epub ahead of print].